

Argonne Preprint PHY-12182-TH-2008

CSSM Preprint ADP-08-10/T670

JLab Preprint JLAB-THY-08-884

**An analysis of the nucleon spectrum from lattice  
partially-quenched QCD**

W. Armour and C. R. Allton

*Department of Physics, Swansea University, Swansea, SA2 8PP, Wales, U.K.*

D. B. Leinweber

*Special Research Centre for the Subatomic Structure of Matter (CSSM),  
School of Chemistry & Physics, University of Adelaide 5005, Australia*

A. W. Thomas

*Jefferson Lab, 12000 Jefferson Ave.,*

*Newport News, VA 23606, USA and*

*College of William and Mary, Williamsburg, VA 23187, USA*

R. D. Young

*Physics Division, Argonne National Laboratory, Argonne, IL 60439, USA*

arXiv:0810.3432v3 [hep-lat] 27 Apr 2010

## Abstract

The chiral extrapolation of the nucleon mass,  $M_n$ , is investigated using data coming from 2-flavour partially-quenched lattice simulations. A large sample of lattice results from the CP-PACS Collaboration is analysed using the leading one-loop corrections, with explicit corrections for finite lattice spacing artifacts. The extrapolation is studied using finite-range regularised chiral perturbation theory. The analysis also provides a quantitative estimate of the leading finite volume corrections. It is found that the discretisation, finite volume and partial quenching effects can all be very well described in this framework, producing an extrapolated value of  $M_n$  in agreement with experiment. Furthermore, determinations of the low energy constants of the nucleon mass's chiral expansion are in agreement with previous methods, but with significantly reduced errors. This procedure is also compared with extrapolations based on polynomial forms, where the results are less encouraging.

## I. INTRODUCTION

There has been great progress in lattice QCD in recent years, associated both with Moore's Law and with improved algorithms, which mean that one can work with larger lattice spacings and still approximate the continuum limit well. The CP-PACS group has devoted considerable effort to the study of the masses of the lowest mass baryons and vector mesons. This has led, for example, to a comprehensive set of data for the mass of the nucleon in partially-quenched QCD (pQQCD), with exceptionally small statistical errors [1]. We shall exploit this data.

The remaining barrier to direct comparison with experimental data is the fact that calculations take much longer as the quark mass approaches the chiral limit. Indeed the time for a given calculation scales somewhere in the range  $m_\pi^{-4}$  to  $m_\pi^{-9}$ , depending on how hard one works to preserve chiral symmetry [2]. As a result there has been considerable interest in using chiral perturbation theory ( $\chi$ PT), an effective field theory (EFT) built on the symmetries of QCD, to provide a functional form for hadron properties as a function of quark mass [3–5]. In principle, such a functional form can then be used to extrapolate from the large pion masses where lattice data exists to the physical value. Unfortunately, there is considerable evidence that the convergence of dimensionally regularised  $\chi$ PT is too slow for this expansion to be reliable at present [6–13].

On the other hand, it can be shown that a reformulation of  $\chi$ PT using finite-range regularisation (FRR) effectively re-sums the chiral expansion, leaving a residual series with much better convergence properties [3, 8]. The FRR expansion is mathematically equivalent to dimensionally regularised  $\chi$ PT to the finite order one is working [8, 14]. Systematic errors associated with the functional form of the regulator are at the fraction of a percent level [3]. A formal description of the formulation of baryon  $\chi$ PT using a momentum cutoff (or FRR) have recently been considered by Djukanovic *et al.* [15]. The price of such an approach is a residual dependence on the regulator mass, which governs the manner in which the loop integrals vanish as the pion mass grows large. However, if it can be demonstrated that reasonable variation of this mass does not significantly change the extrapolated values of physical properties, one has made progress. This seems to be the case for the nucleon mass [11] and magnetic moments [16], for example, where “reasonable variation” is taken to be  $\pm 20\%$  around the best fit value of the regulator mass.

In order to test whether the problem is indeed solved in this way one needs a large body

of accurate data. This is in fact available for the nucleon, where CP-PACS has carried out lattice simulations of pQCD with a wide range of sea and valence masses. This sector requires a modified effective field theory, namely partially-quenched chiral perturbation theory (pQ $\chi$ PT) [17, 18]. Formal developments in this field have made significant progress in the study of a range of hadronic observables — see Refs. [19–21, 24–27], for example.

This large body of pQCD simulation data is analysed within a framework which incorporates the leading low energy behaviour of partially-quenched EFT. Finite-range regularisation is implemented to evaluate loop integrals, for reasons discussed above. The aim is to test whether this approach produces a more satisfactory description of the complete data set than the more commonly used, naive extrapolation formulas.

As we will see, the finite-range regularisation method is able to reproduce the nucleon mass with a remarkable level of accuracy using partially-quenched lattice data at only relatively large pion mass. Furthermore we are able to determine the low energy constants of the chiral expansion of the nucleon mass to a remarkable level of accuracy. For this reason, we encourage the generation of partially-quenched data by the lattice community since it greatly increases the coverage of parameter space, thus enabling chiral extrapolations to the physical point to be performed more accurately.

This work is a companion paper to [28] in which we used the same technique to analyse the vector meson mass, obtaining the  $\rho$ -meson mass to 1% of its physical value.

The next section summarises the finite-range regularised forms for the self-energy of the nucleon in the case of pQCD. Section III discusses the data used from the CP-PACS Collaboration [1]. We then give details of the chiral fits in Sec. IV. Finally, Sec. V reports the consequences of the fits for the determination of the nucleon mass at the physical point.

## II. SELF-ENERGIES FOR THE PARTIALLY-QUENCHED ANALYSIS

Theoretical calculations of dynamical-fermion QCD provide an opportunity to explore the properties of QCD in an expansive manner. The idea is that the sea quark masses (considered in generating the gauge fields of the QCD vacuum) and valence quark masses (associated with operators acting on the QCD vacuum) need not match. Such simulation results are commonly referred to as partially-quenched calculations. Unlike quenched QCD, which connects to full QCD only in the heavy quark limit, pQCD is not an approximation. The chiral coefficients of terms in the chiral expansion (such as the axial couplings of the

$\pi$  and  $\eta'$ ) are the same as in full QCD. Hence, the results of pQQCD provide a theoretical extension of QCD [18]. QCD, as realized in nature, is recovered in the limit where the valence and sea masses match.

In this section we explain the form of the finite-range regularised chiral extrapolation formula in the case of pQQCD — i.e., the case where the valence and sea quarks are not necessarily mass degenerate. This work extends on the early work of Ref. [29], and mirrors our analysis of the vector meson mass in Refs. [28].

We restrict our attention to correlators of nucleons containing three degenerate valence quarks. However, loop diagrams can (and do) contain baryons which contain non-degenerate quarks. For convenience, we introduce the following notation for baryon and pseudoscalar meson masses,  $M_B(\beta, \kappa_{\text{sea}}; \kappa_{\text{val}}^1, \kappa_{\text{val}}^2, \kappa_{\text{val}}^3)$  and  $M_{PS}(\beta, \kappa_{\text{sea}}; \kappa_{\text{val}}^1, \kappa_{\text{val}}^2)$ , where the first two arguments refer to the gauge coupling and sea quark mass, and the arguments after the semi-colon refer to the valence quark values. Throughout the paper it will be convenient to abbreviate this by introducing the notation:

$$\begin{aligned}
M_B^{deg} &= M_B(\beta, \kappa_{\text{sea}}; \kappa_{\text{val}}, \kappa_{\text{val}}, \kappa_{\text{val}}) \\
M_B^{non-deg} &= M_B(\beta, \kappa_{\text{sea}}; \kappa_{\text{sea}}, \kappa_{\text{val}}, \kappa_{\text{val}}) \\
M_{PS}^{deg} &= M_{PS}(\beta, \kappa_{\text{sea}}; \kappa_{\text{val}}, \kappa_{\text{val}}) \\
M_{PS}^{non-deg} &= M_{PS}(\beta, \kappa_{\text{sea}}; \kappa_{\text{sea}}, \kappa_{\text{val}}) \\
M_{PS}^{unit} &= M_{PS}(\beta, \kappa_{\text{sea}}; \kappa_{\text{sea}}, \kappa_{\text{sea}})
\end{aligned} \tag{1}$$

where the superscript *unit* refers to the unitary data; *deg* refers to a hadron containing degenerate valence quarks; and *non-deg* refers to the case where the valence quarks are not degenerate.

The derivation of the pQQCD chiral expansion can be described by diagrammatic methods [21], where the role of sea quark loops in the creation of pseudoscalar meson dressings of the nucleon is easily observed. The self-energy considered below ( $\Sigma_N$ ) is the total contribution from those pion loops which give rise to the leading non-analytic (LNA) and next-to-leading non-analytic (NLNA) terms proportional to  $F$  and  $D$  in the self-energy of the baryon, and also the contributions that arise from the  $\eta'$  diagrams. Explicitly we write the processes as  $N \rightarrow N\pi \rightarrow N$ ,  $N \rightarrow \Delta\pi \rightarrow N$ ,  $N \rightarrow N\eta' \rightarrow N$  and  $N \rightarrow \Delta\eta' \rightarrow N$ . In the limit of full QCD these  $\eta'$  contributions can be neglected because the  $\eta'$  is heavy and therefore decouples from the low energy EFT. The appearance of the unusual term  $N \rightarrow \Delta\eta' \rightarrow N$  is a consequence of the fact that intermediate states in the partially-quenched theory are not

guaranteed to be physical. In particular, the “ $\Delta$ ” here denotes a state of spin-3/2 (but not isospin-3/2) which is degenerate with the corresponding  $\Delta$  state because the hyperfine gluon interaction depends only on the spin of the quark pairs.

For pQCD in the heavy baryon limit the nucleon self-energy may be expressed as:

$$\Sigma_N = \sigma_{NN}^\pi + \sigma_{NN}^{\eta'} + \sigma_{N\Delta}^\pi + \sigma_{N\Delta}^{\eta'} \quad (2)$$

Explicitly we have:

$$\begin{aligned} \sigma_{NN}^\pi &= -\frac{3(F+D)^2}{32\pi f_\pi^2} \left( I(M_{PS}^{deg}, 0) \right. \\ &\quad \left. + \alpha (I(M_{PS}^{non-deg}, M_N^{non-deg} - M_N^{deg}) - I(M_{PS}^{deg}, 0)) \right) \\ \sigma_{NN}^{\eta'} &= -\frac{(3F-D)^2}{32\pi f_\pi^2} \left( ((M_{PS}^{deg})^2 - (M_{PS}^{unit})^2) I_2(M_{PS}^{deg}) \right. \\ &\quad \left. + \beta (I(M_{PS}^{non-deg}, M_N^{non-deg} - M_N^{deg}) - I(M_{PS}^{deg}, 0)) \right) \\ \sigma_{N\Delta}^\pi &= -\frac{1}{32\pi f_\pi^2} \frac{8}{3} \gamma^2 \left( \frac{5}{8} I(M_{PS}^{deg}, M_\Delta^{deg} - M_N^{deg}) \right. \\ &\quad \left. + \frac{3}{8} I(M_{PS}^{non-deg}, M_\Delta^{non-deg} - M_N^{deg}) \right) \\ \sigma_{N\Delta}^{\eta'} &= -\frac{1}{32\pi f_\pi^2} \frac{1}{3} \gamma^2 \left( I(M_{PS}^{non-deg}, M_\Delta^{non-deg} - M_N^{deg}) \right. \\ &\quad \left. - I(M_{PS}^{deg}, M_\Delta^{deg} - M_N^{deg}) \right) \end{aligned} \quad (3)$$

As we will see (fig.3),  $\sigma_{NN}^\pi$  and  $\sigma_{N\Delta}^\pi$  are typically negative, whereas  $\sigma_{NN}^{\eta'}$  and  $\sigma_{N\Delta}^{\eta'}$  are typically around zero. The parameters  $\alpha$ ,  $\beta$  &  $\gamma$  are derived from the standard  $SU(6)$  couplings [38].

Explicitly we take

$$\begin{aligned} \alpha &= \frac{\Gamma}{2(F+D)^2} \\ \beta &= \frac{\Gamma}{2(3F-D)^2} \\ \gamma &= -2D \\ \Gamma &= \frac{1}{3}(3F+D)^2 + 3(D-F)^2 \end{aligned} \quad (4)$$

We use the constants  $F = 0.51$  and  $D = 0.76$ , which are determined from fitting semi-leptonic decays at tree level— e.g., Ref. [32].

The integrals in eq.(3) are defined as

$$\begin{aligned} I(M_{PS}, \delta M) &= \frac{2}{\pi} \int_0^\infty \frac{k^4 u^2(k) dk}{\omega(\omega + \delta M)} \\ I_2(M_{PS}) &= \frac{2}{\pi} \int_0^\infty \frac{k^4 u^2(k) dk}{\omega^4}, \end{aligned} \quad (5)$$

where we have used:

$$\omega(k) = \sqrt{k^2 + M_{PS}^2} \quad (6)$$

Here  $M_{PS}$  can be  $M_{PS}^{deg}$  or  $M_{PS}^{non-deg}$ . We define this along with values for  $\delta M$  explicitly in the individual self-energy terms above.

We study both a standard dipole form factor, which takes the form

$$u(k) = \frac{\Lambda^4}{(\Lambda^2 + k^2)^2}, \quad (7)$$

and a Gaussian form factor

$$u(k) = \exp\left(-\frac{k^2}{\Lambda^2}\right). \quad (8)$$

To account for finite volume artefacts, the self-energy equations are discretised so that only those momenta allowed on the lattice appear:

$$4\pi \int_0^\infty k^2 dk = \int d^3k \approx \frac{1}{V} \left(\frac{2\pi}{a}\right)^3 \sum_{k_x, k_y, k_z}, \quad (9)$$

with

$$k_{x,y,z} = \frac{2\pi(i, j, k)}{aN_{x,y,z}}. \quad (10)$$

with  $i, j, k \in \mathcal{Z}$ . The purpose of the finite-range regulator is to regularise the theory as  $k_x, k_y, k_z$  tend to infinity. Indeed, once any one of  $k_x, k_y$  or  $k_z$  is greater than  $\sim 10\Lambda$  the contribution to the integral is negligible and thereby ensuring convergence of the summation. Hence, we would like the highest momentum in each direction to be just over  $10\Lambda$ . For practical calculation, we therefore use the following to calculate the maxima and minima for  $i, j, k$ :

$$\begin{aligned} (i, j, k)_{max} &= \left\lceil \frac{10\Lambda a}{2\pi} N_{(x,y,z)} \right\rceil + 1, \\ (i, j, k)_{min} &= - \left\lfloor \frac{10\Lambda a}{2\pi} N_{(x,y,z)} \right\rfloor - 1, \end{aligned}$$

where  $[\dots]$  denotes the integer part.

We now have the partially-quenched nucleon mass formula which we will use in sec. IV to fit the CP-PACS data.

$\beta$	$\kappa_{sea}$	Volume	$M_{PS}^{unit}/M_V^{unit}$	$a_{r_0}$ [fm]	$a_\sigma$ [fm]
1.80	0.1409	$12^3 \times 24$	$0.8067_{-9}^{+9}$	$0.286_{-6}^{+6}$	$0.288_{-3}^{+3}$
1.80	0.1430	$12^3 \times 24$	$0.7526_{-15}^{+16}$	$0.272_{-2}^{+2}$	$0.280_{-5}^{+4}$
1.80	0.1445	$12^3 \times 24$	$0.694_{-2}^{+2}$	$0.258_{-4}^{+4}$	$0.269_{-3}^{+2}$
1.80	0.1464	$12^3 \times 24$	$0.547_{-4}^{+4}$	$0.237_{-4}^{+4}$	$0.248_{-3}^{+2}$
1.95	0.1375	$16^3 \times 32$	$0.8045_{-11}^{+11}$	$0.196_{-4}^{+4}$	$0.2044_{-12}^{+10}$
1.95	0.1390	$16^3 \times 32$	$0.752_{-2}^{+2}$	$0.185_{-3}^{+3}$	$0.1934_{-15}^{+14}$
1.95	0.1400	$16^3 \times 32$	$0.690_{-2}^{+2}$	$0.174_{-2}^{+2}$	$0.1812_{-12}^{+12}$
1.95	0.1410	$16^3 \times 32$	$0.582_{-3}^{+3}$	$0.163_{-2}^{+2}$	$0.1699_{-15}^{+13}$
2.10	0.1357	$24^3 \times 48$	$0.806_{-2}^{+2}$	$0.1275_{-5}^{+5}$	$0.1342_{-8}^{+8}$
2.10	0.1367	$24^3 \times 48$	$0.755_{-2}^{+2}$	$0.1203_{-5}^{+4}$	$0.1254_{-8}^{+8}$
2.10	0.1374	$24^3 \times 48$	$0.691_{-3}^{+3}$	$0.1157_{-4}^{+4}$	$0.1203_{-6}^{+6}$
2.10	0.1382	$24^3 \times 48$	$0.576_{-4}^{+3}$	$0.1093_{-3}^{+3}$	$0.1129_{-5}^{+4}$
2.20	0.1351	$24^3 \times 48$	$0.799_{-3}^{+3}$	$0.0997_{-5}^{+4}$	$0.10503_{-15}^{+15}$
2.20	0.1358	$24^3 \times 48$	$0.753_{-4}^{+4}$	$0.0966_{-4}^{+4}$	$0.1013_{-2}^{+3}$
2.20	0.1363	$24^3 \times 48$	$0.705_{-6}^{+6}$	$0.0936_{-4}^{+4}$	$0.0978_{-3}^{+3}$
2.20	0.1368	$24^3 \times 48$	$0.632_{-8}^{+8}$	$0.0906_{-4}^{+4}$	$0.0949_{-2}^{+2}$

TABLE I: The lattice parameters of the CP-PACS simulation used in this data analysis, taken from Ref. [1]. The superscript *unit* refers to the unitary data (i.e., where  $\kappa_{val}^1 \equiv \kappa_{val}^2 \equiv \kappa_{sea}$ ). Note that the errors reported in this table are obtained with our bootstrap ensembles (see text).

### III. THE CP-PACS NUCLEON DATA

In Ref. [1], the CP-PACS collaboration published meson and baryon spectrum data from dynamical simulations for mean-field improved Wilson fermions with improved gluons at four different  $\beta$  values. For each value of  $\beta$ , ensembles were generated for four values of  $\kappa_{sea}$  – giving a total of 16 independent ensembles. Table I summarises the lattice parameters used and Figure 1 is a graphical representation of the unitary pseudo-scalar masses plotted against the lattice spacing  $a_{r_0}$  and we note that  $(M_{PS}^{unit})^2$  is a direct measure of the sea quark mass. For each of the sixteen ensembles there are five  $\kappa_{val}$  values considered [1]. Thus there are a total of 80  $(M_N^{deg}, M_{PS}^{deg})$  data points available for analysis.



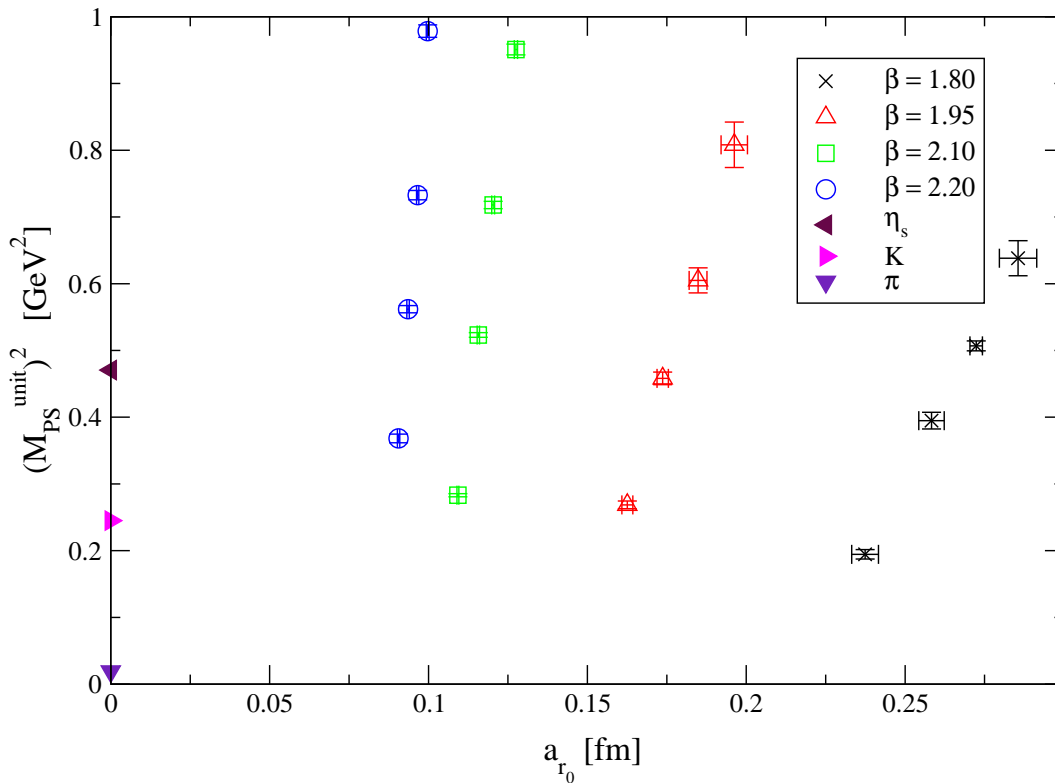


FIG. 1: The range of sea quark mass  $(M_{PS}^{unit})^2$  and lattice spacing,  $a_{r_0}$ , covered by the CP-PACS data displayed in Table I.  $(M_{PS}^{unit})^2$  is the pseudoscalar meson mass squared at the unitary point; i.e., where  $\kappa_{val} \equiv \kappa_{sea}$ . The experimental points for the  $\pi$ ,  $K$  and “ $\eta_s$ ” mesons are also shown for reference.

The analysis in this paper shares many common features with our analysis of the vector meson data in Ref. [28]. In particular, we consider two methods of setting the scale: the string tension ( $\sigma$ ), and the hadronic scale ( $r_0$ ). We generate 1000 bootstrap clusters for all hadronic masses from a Gaussian distribution with a central value equal to the values published in [1] (tables XXI, XXII and XXIII [39]) and a FWHM equal to the published error. We use totally uncorrelated data throughout, which we argue in Ref. [28] leads to our statistical errors being overestimates. The values  $r_0 = 0.49$  fm and  $\sqrt{\sigma} = 440$  MeV are used.

Since the action used in [1] is mean-field, rather than non-perturbatively improved, it will have some residual lattice systematic errors of  $\mathcal{O}(a)$ . We therefore fit the data assuming both  $\mathcal{O}(a)$  and  $\mathcal{O}(a^2)$  effects, which we investigate in Sec. IV.

The physical volume for the  $\beta = 1.80, 1.95$  and  $2.10$  ensembles is  $La \approx 2.5$  fm, and the  $\beta = 2.20$  ensemble has a slightly smaller physical volume. The associated finite volume effects

are incorporated through evaluating the chiral loops by explicitly summing the discrete pion momenta allowed on the lattice as described in eq.(9).

## IV. FITTING ANALYSIS

### A. Summary of analysis techniques

The philosophy behind our fitting method remains the same as for our investigation of the meson spectrum [28], i.e. we work in physical units when performing our extrapolations. We do this so that data from different ensembles can be combined; something which cannot be done for the dimensionless data since they correspond to differing lattice spacings. In addition, we expect that this approach will benefit from some cancellation of the systematic (and statistical) errors.

The Adelaide approach to chiral fits describes the variation of hadron mass with quark mass by a combination of the self-energy term (in this case,  $\Sigma_N$ ) with “constituent quark” terms (i.e. polynomials in the *valence* quark mass). The former accurately describe the chiral behaviour and become negligible as the quark mass becomes heavy. Thus we have

$$M_N - \Sigma_N = a_0 + a_2(M_{PS}^{deg})^2 + a_4(M_{PS}^{deg})^4 + a_6(M_{PS}^{deg})^6. \quad (11)$$

In the complete EFT for the partially-quenched theory, there are contributions to this polynomial expansion which measure the displacement from the unitarity point (where  $m_{val} = m_{sea}$ ). This freedom could be incorporated by extending the terms polynomial in the quark mass by

$$\begin{aligned} a_2(M_{PS}^{deg})^2 &\rightarrow a_2(M_{PS}^{deg})^2 + a'_2\delta_{vs}^2, \\ a_4(M_{PS}^{deg})^4 &\rightarrow a_4(M_{PS}^{deg})^4 + a'_4(M_{PS}^{deg})^2\delta_{vs}^2 + a''_4\delta_{vs}^4, \end{aligned} \quad (12)$$

and similarly for the third-order term. Here, the notation  $\delta_{vs}^2 = (M_{PS}^{deg})^2 - (M_{PS}^{unit})^2$  is used to describe the mass splitting between the sea and valence quarks. In line with our earlier work, Ref. [28], we make a model assumption by ignoring the terms proportional to  $\delta_{vs}^2$ . We have checked this assumption by confirming numerically that there is no variation of the  $a_2$  coefficient (obtained with the “individual ensemble fit” approach — see next subsection) with  $M_{PS}^{unit}$ . We found a similar situation in our earlier work, Ref. [28]. In any case, any dependencies below the level of our statistics on  $\delta_{vs}^2$  are implicitly contained within the chiral

self-energies,  $\Sigma_N$ . Thereby, we use the lattice data to select a preferential regularisation scale (and perhaps regulator) which efficiently interpolates between the partially-quenched and unitary points. This method has proven very successful in connecting quenched and dynamical QCD results over a range of observables, see Refs. [16, 22, 23, 30] for example. In effect, the 6 new parameters (at this order) characterising the non-unitarity dependence are modelled by a single parameter  $\Lambda$ .

Again, following our vector-meson analysis [28], we contrast this chirally-motivated approach with a naive polynomial fitting function,

$$M_N = a_0 + a_2(M_{PS}^{deg})^2 + a_4(M_{PS}^{deg})^4 + a_6(M_{PS}^{deg})^6. \quad (13)$$

We divide these fits into two categories, ‘‘cubic’’ and ‘‘quadratic’’ depending on whether or not the  $(M_{PS}^{deg})^6$  is included.

In fig. 2 we plot the dimensionful nucleon data,  $M_N$ , and the subtracted nucleon data,  $M_N - \Sigma_N$ . In the latter, we use a representative value of  $\Lambda = 600$  MeV with the dipole form factor and the scale set by  $r_0$ .

We plot, in fig. 3, the terms which make up  $\Sigma_N$  (see eq.(2)) for each of the 80 data points under consideration, in order to get a feel for their relative size. We also show the continuum, physical values for these terms, noting that in this case, the terms involving  $\eta'$  vanish (as required). The curvature in the terms which make up  $\Sigma_N$  seen in fig. 3 as  $M_{PS} \rightarrow 0$  matches, by design, the LNA and NLNA chiral contributions (see sec.II). The polynomial chiral fits obviously do not reproduce this chiral behaviour. It is this curvature which means that the Adelaide approach more accurately reproduces the experimental value of the nucleon mass than the naive polynomial approach, predicting a nucleon mass some 60MeV lower than the polynomial approach (see later).

In the next subsection we individually fit Eqs. (11 & 13) to the sixteen ensembles (Table I). Following this we perform a single global fit of the entire data set using Eqs. (11 & 13) modified appropriately by  $\mathcal{O}(a)$ -style corrections.

## B. Individual ensemble fits

In this section we treat the sixteen ensembles separately by fitting Eqs.(11 & 13) to the five degenerate data points  $(M_N^{deg}, M_{PS}^{deg})$  from each of the sixteen ensembles. In the Adelaide case, we have used our preferred choices of the dipole form factor with the scale taken from

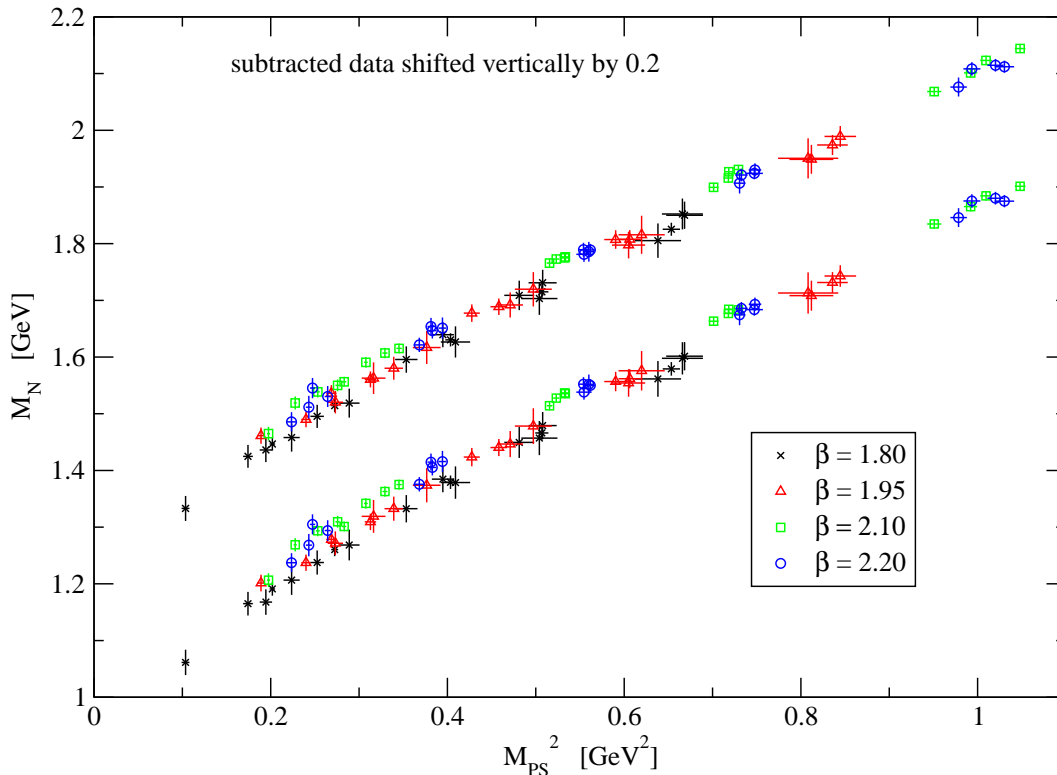


FIG. 2: A plot of the degenerate CP-PACS nucleon data set. Here the scale is set using  $r_0$ . Both the raw data,  $M_N$ , and the subtracted data,  $M_N - \Sigma_N$ , are shown, with the latter shifted vertically by 0.2 GeV for clarity. A dipole form factor with  $\Lambda = 600$  MeV was chosen in the latter case.

$r_0$ . The other possibilities (i.e., using the Gaussian form factor and taking the scale from the string tension) are discussed in Sec. IV C. We have chosen  $\Lambda = 600$  MeV for these individual fits which is very close to what turns out to be our preferred value in Sec. IV C. (Section IV C discusses in detail the variation of nucleon mass with  $\Lambda$ .) The fits considered in this section are quadratic in the chiral expansion (i.e., we set  $a_6 = 0$  in Eqs. (11 & 13)) since cubic fits for the individual fits have 100% error in the  $a_4$  and  $a_6$  coefficients.

Table II lists the coefficients for both the Adelaide fits and also the naive fits using this approach. As expected the leading Adelaide coefficient is always greater than the corresponding coefficient from the naive fits ( $a_0^{adel} > a_0^{naive}$ ). In virtually all cases the  $a_2$  coefficient is smaller for the Adelaide fits ( $a_2^{adel} < a_2^{naive}$ ). The  $a_4$  coefficients are approximately the same for both fits ( $a_4^{adel} \sim a_4^{naive}$ ), but the error in this coefficient is very large, typically 50%. We see only that the  $a_4$  coefficient is zero within errors in only one ensemble, indicating its presence is needed.

$\beta$	$\kappa_{sea}$	$a_0^{naive}$ [GeV]	$a_0^{adel}$ [GeV]	$a_2^{naive}$ [GeV <sup>-1</sup> ]	$a_2^{adel}$ [GeV <sup>-1</sup> ]	$a_4^{naive}$ [GeV <sup>-3</sup> ]	$a_4^{adel}$ [GeV <sup>-3</sup> ]
1.80	0.1409	0.97 <sup>+4</sup> <sub>-4</sub>	1.03 <sup>+4</sup> <sub>-4</sub>	1.11 <sup>+12</sup> <sub>-14</sub>	1.09 <sup>+13</sup> <sub>-14</sub>	-0.30 <sup>+15</sup> <sub>-13</sub>	-0.29 <sup>+15</sup> <sub>-14</sub>
1.80	0.1430	0.98 <sup>+3</sup> <sub>-2</sub>	1.04 <sup>+3</sup> <sub>-2</sub>	1.11 <sup>+11</sup> <sub>-12</sub>	1.08 <sup>+11</sup> <sub>-12</sub>	-0.29 <sup>+13</sup> <sub>-12</sub>	-0.29 <sup>+13</sup> <sub>-13</sub>
1.80	0.1445	0.96 <sup>+3</sup> <sub>-3</sub>	1.03 <sup>+3</sup> <sub>-3</sub>	1.21 <sup>+12</sup> <sub>-11</sub>	1.18 <sup>+13</sup> <sub>-12</sub>	-0.37 <sup>+13</sup> <sub>-14</sub>	-0.37 <sup>+13</sup> <sub>-14</sub>
1.80	0.1464	0.93 <sup>+3</sup> <sub>-3</sub>	1.01 <sup>+3</sup> <sub>-3</sub>	1.27 <sup>+12</sup> <sub>-10</sub>	1.23 <sup>+12</sup> <sub>-11</sub>	-0.42 <sup>+12</sup> <sub>-14</sub>	-0.41 <sup>+12</sup> <sub>-14</sub>
1.95	0.1375	1.00 <sup>+4</sup> <sub>-3</sub>	1.05 <sup>+4</sup> <sub>-3</sub>	1.08 <sup>+10</sup> <sub>-12</sub>	1.07 <sup>+11</sup> <sub>-12</sub>	-0.25 <sup>+10</sup> <sub>-8</sub>	-0.25 <sup>+10</sup> <sub>-9</sub>
1.95	0.1390	1.00 <sup>+3</sup> <sub>-2</sub>	1.06 <sup>+3</sup> <sub>-2</sub>	1.04 <sup>+8</sup> <sub>-8</sub>	1.02 <sup>+8</sup> <sub>-8</sub>	-0.21 <sup>+7</sup> <sub>-7</sub>	-0.20 <sup>+7</sup> <sub>-7</sub>
1.95	0.1400	0.99 <sup>+2</sup> <sub>-2</sub>	1.05 <sup>+2</sup> <sub>-2</sub>	1.11 <sup>+7</sup> <sub>-7</sub>	1.08 <sup>+7</sup> <sub>-7</sub>	-0.26 <sup>+6</sup> <sub>-6</sub>	-0.25 <sup>+6</sup> <sub>-6</sub>
1.95	0.1410	1.01 <sup>+2</sup> <sub>-2</sub>	1.07 <sup>+2</sup> <sub>-2</sub>	1.08 <sup>+7</sup> <sub>-6</sub>	1.05 <sup>+7</sup> <sub>-6</sub>	-0.24 <sup>+6</sup> <sub>-6</sub>	-0.23 <sup>+6</sup> <sub>-7</sub>
2.10	0.1357	1.04 <sup>+2</sup> <sub>-2</sub>	1.08 <sup>+2</sup> <sub>-2</sub>	1.06 <sup>+7</sup> <sub>-7</sub>	1.05 <sup>+7</sup> <sub>-7</sub>	-0.23 <sup>+5</sup> <sub>-5</sub>	-0.23 <sup>+5</sup> <sub>-5</sub>
2.10	0.1367	1.05 <sup>+2</sup> <sub>-2</sub>	1.10 <sup>+2</sup> <sub>-2</sub>	1.01 <sup>+7</sup> <sub>-7</sub>	0.99 <sup>+7</sup> <sub>-7</sub>	-0.19 <sup>+5</sup> <sub>-5</sub>	-0.19 <sup>+5</sup> <sub>-5</sub>
2.10	0.1374	1.04 <sup>+2</sup> <sub>-2</sub>	1.10 <sup>+2</sup> <sub>-2</sub>	1.03 <sup>+7</sup> <sub>-7</sub>	1.01 <sup>+7</sup> <sub>-7</sub>	-0.19 <sup>+5</sup> <sub>-5</sub>	-0.19 <sup>+5</sup> <sub>-5</sub>
2.10	0.1382	1.00 <sup>+2</sup> <sub>-2</sub>	1.06 <sup>+2</sup> <sub>-2</sub>	1.13 <sup>+6</sup> <sub>-6</sub>	1.10 <sup>+6</sup> <sub>-6</sub>	-0.25 <sup>+4</sup> <sub>-4</sub>	-0.25 <sup>+4</sup> <sub>-4</sub>
2.20	0.1351	1.04 <sup>+5</sup> <sub>-5</sub>	1.08 <sup>+5</sup> <sub>-5</sub>	1.0 <sup>+2</sup> <sub>-2</sub>	1.0 <sup>+2</sup> <sub>-2</sub>	-0.21 <sup>+12</sup> <sub>-15</sub>	-0.21 <sup>+13</sup> <sub>-15</sub>
2.20	0.1358	1.10 <sup>+4</sup> <sub>-4</sub>	1.14 <sup>+4</sup> <sub>-4</sub>	0.87 <sup>+12</sup> <sub>-13</sub>	0.86 <sup>+12</sup> <sub>-14</sub>	-0.09 <sup>+10</sup> <sub>-9</sub>	-0.08 <sup>+10</sup> <sub>-9</sub>
2.20	0.1363	1.04 <sup>+4</sup> <sub>-4</sub>	1.08 <sup>+4</sup> <sub>-4</sub>	1.03 <sup>+13</sup> <sub>-11</sub>	1.01 <sup>+13</sup> <sub>-12</sub>	-0.20 <sup>+8</sup> <sub>-9</sub>	-0.19 <sup>+8</sup> <sub>-9</sub>
2.20	0.1368	1.01 <sup>+4</sup> <sub>-3</sub>	1.06 <sup>+4</sup> <sub>-3</sub>	1.08 <sup>+11</sup> <sub>-11</sub>	1.05 <sup>+11</sup> <sub>-11</sub>	-0.23 <sup>+8</sup> <sub>-8</sub>	-0.22 <sup>+8</sup> <sub>-8</sub>

TABLE II: The coefficients obtained from fitting  $M_N$  data against  $M_{PS}^2$ . We list results for both the naive and Adelaide fits ( Eqs. (13) & (11), respectively) for each of the sixteen ensembles listed in Table I. A dipole form factor was employed for the Adelaide fits using  $\Lambda = 600$  [MeV] and the scale was set from  $r_0$ .

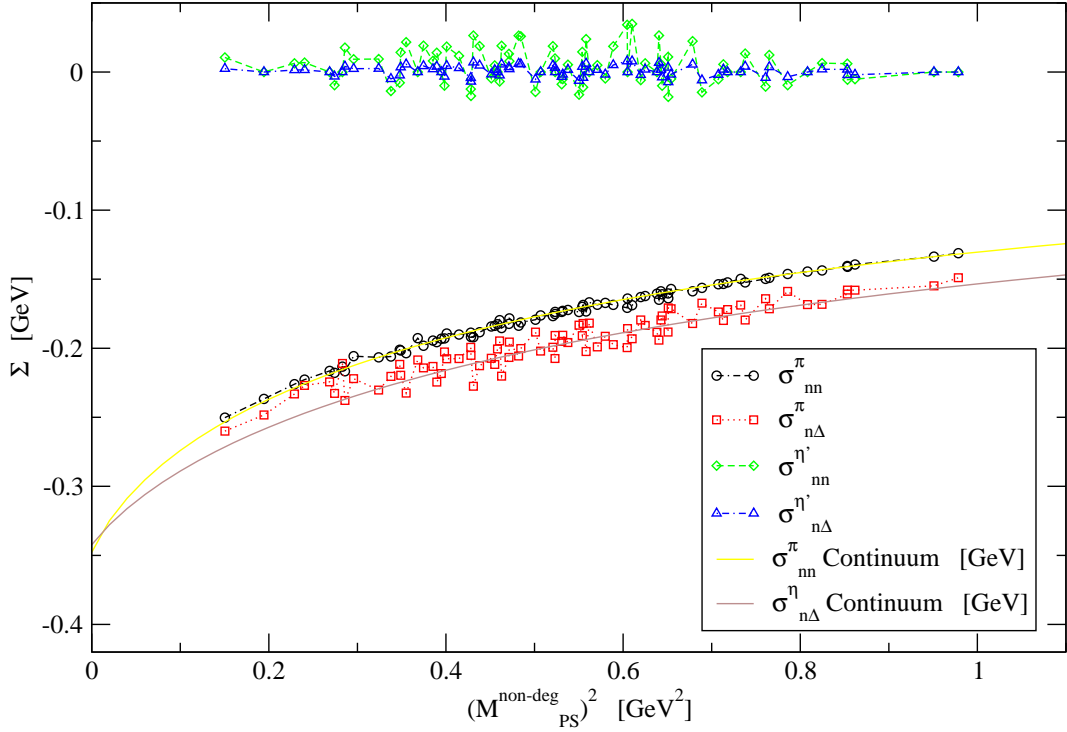


FIG. 3: Here we plot the self-energy contributions Eqs. 3) versus  $(M_{PS}^{non-deg})^2$  for the entire degenerate data set (dashed lines are a guide for the eye only). We use the dipole form factor and choose an arbitrary value for the Lambda parameter,  $\Lambda = 1$  [GeV]. We also include continuum, physical data (the solid curves) for the pion processes (the  $\eta$  case vanishes in the physical limit).

Figure 4 is a representative example of one of these fits. It corresponds to the  $(\beta, \kappa_{sea}) = (2.10, 0.1382)$  ensemble, which is one of closest to the physical point ( fig. 1).

With a view to performing a combined, global fit to all sixteen ensembles, we note from Table II that there appears to be no discernible trend with the sea quark mass for any of the chiral coefficients. However, there does appear to be a lattice spacing effect. Figures (5 & 6) plot  $a_{0,2}$  against the lattice spacing from  $r_0$ ,  $a_{r_0}$ . These plots motivate the following continuum extrapolation

$$a_{0,2} = a_{0,2}^{cont} + X_{0,2}^{individual} a_{r_0}. \quad (14)$$

(Note that in sec. IV C we investigate both  $\mathcal{O}(a)$  and  $\mathcal{O}(a^2)$  corrections to the chiral coefficients.) The results of the fits corresponding to Eq. (14) are listed in Table III.

We note that the errors in the  $X_0^{individual}$  coefficients are around 25%, whereas they are more than 50% for  $X_2^{individual}$ .

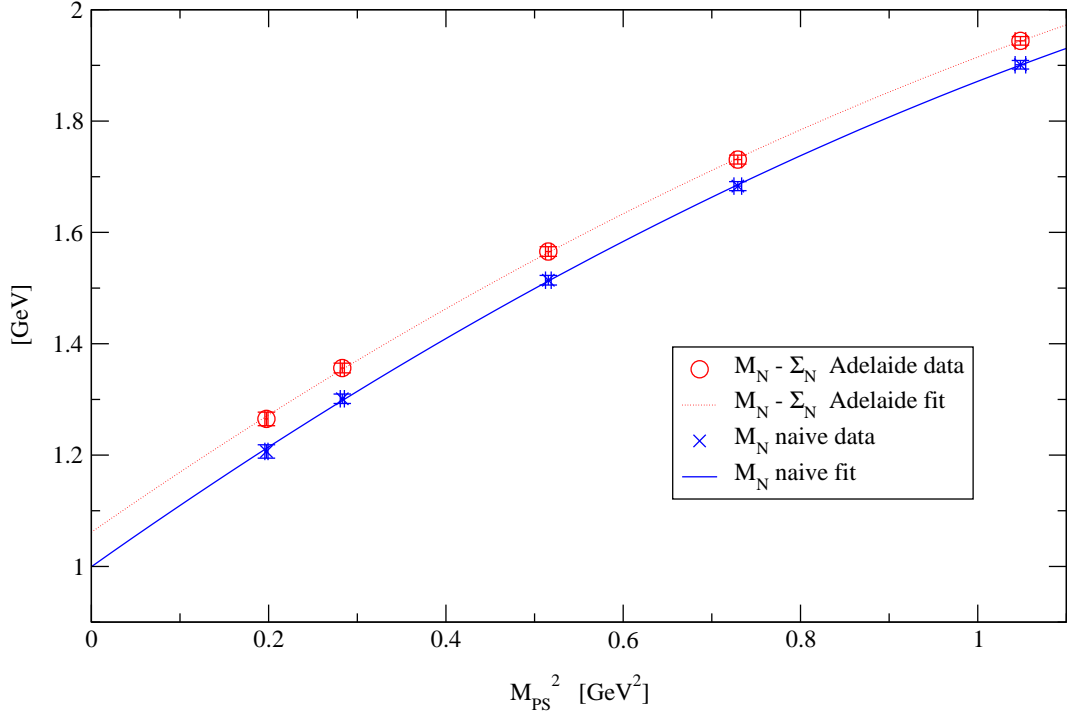


FIG. 4: A plot of  $M_N$  versus  $M_{PS}^2$  for the ensemble  $(\beta, \kappa_{\text{sea}}) = (2.10, 0.1382)$ . Included are the results of the quadratic naive, Eq. (13) and the quadratic Adelaide, eq.(11) fits. The scale is set from  $r_0$ , we use a dipole form factor and our preferred value for  $\Lambda$  ( $\Lambda = 600$  [MeV]).

	$a_0^{cont.}$ [GeV]	$X_0^{individual}$ [GeV/fm]	$\chi_0^2/d.o.f.$	$a_2^{cont.}$ [GeV <sup>-1</sup> ]	$X_2^{individual}$ [GeV <sup>-1</sup> /fm]	$\chi_2^2/d.o.f.$
Naive-fit	$1.08_{-2}^{+2}$	$-0.44_{-11}^{+10}$	13 / 14	$0.97_{-6}^{+7}$	$0.7_{-4}^{+4}$	7 / 14
Adelaide-fit	$1.12_{-2}^{+2}$	$-0.37_{-11}^{+10}$	8 / 14	$0.96_{-6}^{+7}$	$0.6_{-4}^{+4}$	6 / 14

TABLE III: The coefficients obtained from the continuum extrapolation of both the naive and Adelaide  $a_{0,2}$  values from Table II using Eq. (14).

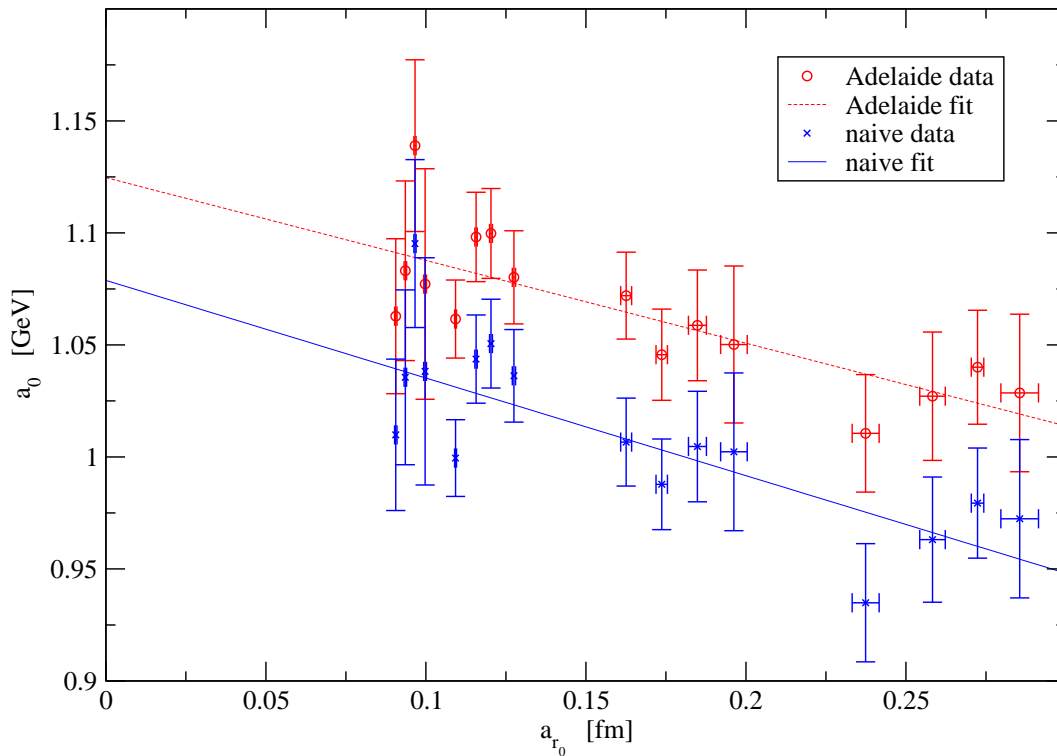


FIG. 5: A continuum extrapolation of the  $a_0$  coefficient obtained from both the Adelaide and naive fits Eq. (14).

### C. Global fits

We now analyse the complete set of 80  $(M_{PS}, M_N)$  data points by globally fitting the sixteen ensembles of Table I. As in Ref. [28], the idea is that this will produce a highly constrained fit and allow us to determine the higher order coefficients in the chiral expansion in Eqs.(11 & 13), the Adelaide scale parameter,  $\Lambda$ , and the preferred form factor.

In order to combine data from different ensembles into a single fit, we use the experience gained in sec. IV B and in Refs. [28]. This tells us that the data's lattice spacing artifacts, which are sizable enough for us to discern, lie in the leading coefficient,  $a_0$ . We have checked this conclusion by studying combinations of  $\mathcal{O}(a)$  and  $\mathcal{O}(a^2)$  terms [40] in the  $a_2$  and higher coefficients, but have found that these fits are unstable. Therefore our global fitting functions for the Adelaide case is a modified version of Eq. (11):

$$M_N - \Sigma_N = (a_0 + X_n a^n) + a_2 (M_{PS}^{deg})^2 + a_4 (M_{PS}^{deg})^4 + a_6 (M_{PS}^{deg})^6 \quad (15)$$



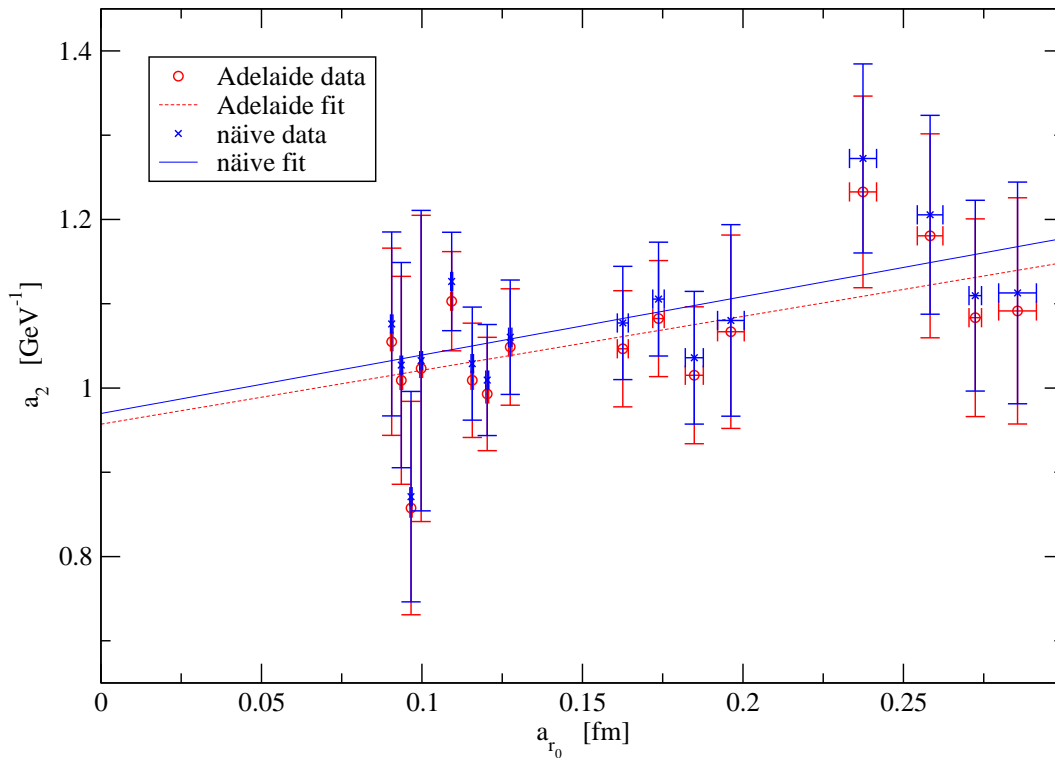


FIG. 6: A continuum extrapolation of the  $a_2$  coefficient obtained from both the Adelaide and naive fits Eq. (14).

and the global fit function corresponding to the naive case Eq. (13) is

$$M_N = (a_0 + X_n a^n) + a_2 (M_{PS}^{deg})^2 + a_4 (M_{PS}^{deg})^4 + a_6 (M_{PS}^{deg})^6 \quad (16)$$

We consider both “quadratic” and “cubic” chiral fits and also consider both  $\mathcal{O}(a)$  and  $\mathcal{O}(a^2)$  lattice spacing effects in the  $a_0$  coefficient. Hence, for the global fit analysis the maximum number of fit parameters in any one fitting function is five. (We discuss the  $\Lambda$  parameter in the Adelaide case later.) Since our data set contains 80 points, the fit will hopefully provide highly constrained fit parameters compared to those from the individual fitting method (see Table II). The scale was set using both the string tension and Sommer scale,  $r_0$ . Finally, for the Adelaide method we study both the dipole, Eq. (7), and Gaussian, Eq. (8) form factors.

The different choices of fitting procedure are summarised in Table IV. In this table, the entries in each column represent a separate possibility, making making a total of  $2^4$  Adelaide and  $2^3$  naive fitting types.

When performing the Adelaide fits, we have to set the  $\Lambda$  value, see Eqs. (7,8). For

Fit	Chiral	$\mathcal{O}(a^n)$	Lattice
Approach	Extrapolation	term in $a_0$	Spacing from:
Adelaide - Dipole	Cubic	$\mathcal{O}(a)$	$r_0$
Adelaide - Gaussian	Quadratic	$\mathcal{O}(a^2)$	$\sigma$
Naive			

TABLE IV: The different fit types used in the global analysis.

numerical reasons, we chose a set of trial  $\Lambda$  values, rather than let it be a free parameter in the fitting procedure. In figs. 7 and 8, we show the  $\chi^2/d.o.f.$  versus  $\Lambda$  for each of the fitting choices in the Adelaide case, for the dipole and Gaussian form factors, respectively. This allows us to study the quality of the fits as a function of  $\Lambda$  and to fix the best value of  $\Lambda$  for these fits.

From figs. 7 and 8, we see that the behaviour of  $\chi^2$  versus  $\Lambda$  is not very dependent on either how the lattice spacing effects in the  $a_0$  coefficient are modelled or on the order of chiral expansion. Note also that the best  $\Lambda$  value, (i.e., the one which minimises  $\chi^2$ ) does not appear to depend on how the lattice spacing effects are modelled. Changing the form factor from dipole to Gaussian results in very similar  $\chi^2$  behaviour, except that the  $\Lambda$  value is simply shifted and the dipole gives a slightly lower  $\chi^2$ . The biggest effect on the  $\chi^2/d.o.f.$  versus  $\Lambda$  curves is the choice of whether one uses  $r_0$  or  $\sigma$  to set the scale, with  $r_0$  clearly producing the best fits.

For each of the Adelaide fit choices we have determined the “best”  $\Lambda$  value, i.e., the one which minimises the  $\chi^2$ . These are listed in Table V. We use these values of  $\Lambda$  to perform the sixteen Adelaide fits in Table IV. The results of these fits, together with the eight naive fits, are listed in Tables VI and VII, where the scale is set by  $r_0$  and  $\sigma$ , respectively.

We summarise the results of Tables VI and VII below.

- *Fit approach*

We see that the smallest  $\chi^2/d.o.f.$  (indicating the best fitting procedure) is given by the Adelaide method which uses a dipole form factor. This has the best  $\chi^2/d.o.f.$  in *every* case (independent of how the chiral extrapolation was truncated, how the lattice

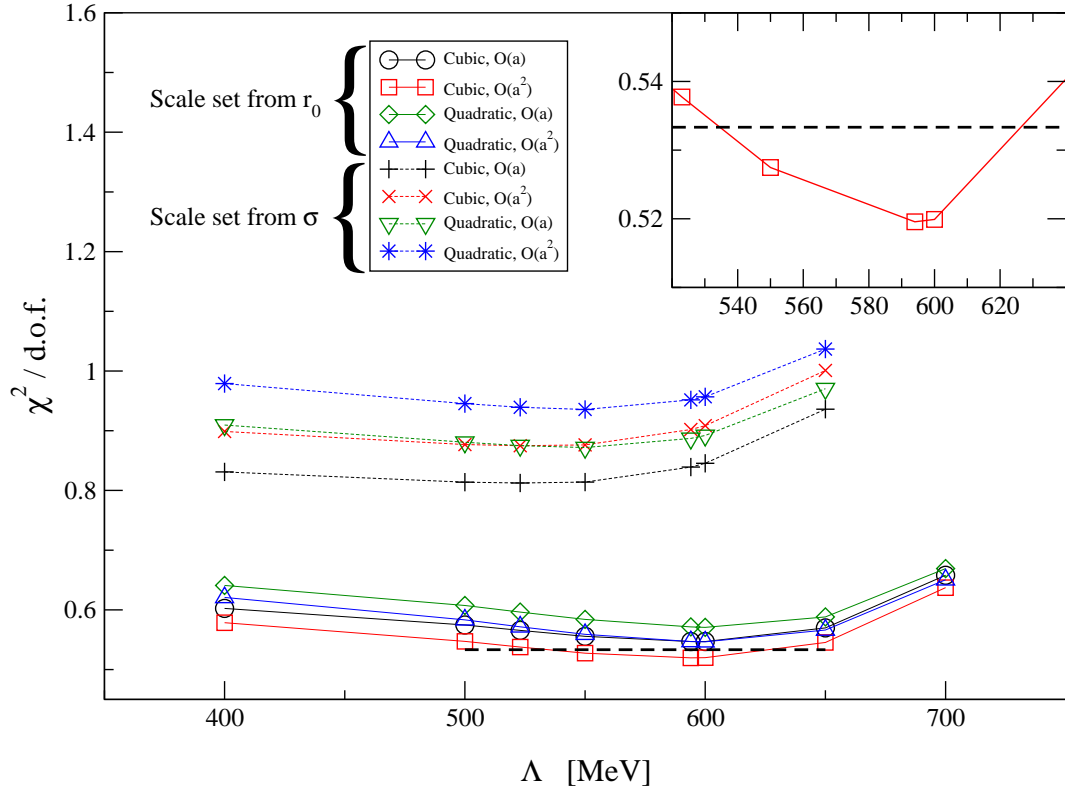


FIG. 7: A plot of  $\chi^2/d.o.f$  against  $\Lambda$  for the dipole form factor. The dashed horizontal line represents increasing  $\chi^2$  from its minimum value by unity for the  $r_0$  data (i.e. it represents one standard deviation). The intercept of this dashed line with the  $\chi^2$  curves (at  $\Lambda = 535$  and  $626$  MeV) is used to derive upper and lower bounds for the preferred  $\Lambda$  value for the dipole case.

artefacts in  $a_0$  were modelled and how the spacing was set). Using the Gaussian form factor leads to poorer  $\chi^2$  values which are similar to, or worse than the naive approach.

- *Chiral extrapolation*

Errors in the cubic chiral coefficient are large compared to their quadratic counterparts. However, the cubic fits always produce a non-zero  $a_6$  coefficient and they also lead to a smaller  $\chi^2$  value than the corresponding quadratic fits. This indicates the need for a cubic chiral term. (Note that quadratic chiral fits were preferred in the mesonic case [28].)

- *Treatment of the lattice spacing systematics and the fit coefficients*

We see that the fits with  $\mathcal{O}(a^2)$  rather than  $\mathcal{O}(a)$  lead to a lower  $\chi^2$  in the  $r_0$  case, whereas the reverse is true when the string tension is used to set the scale. This

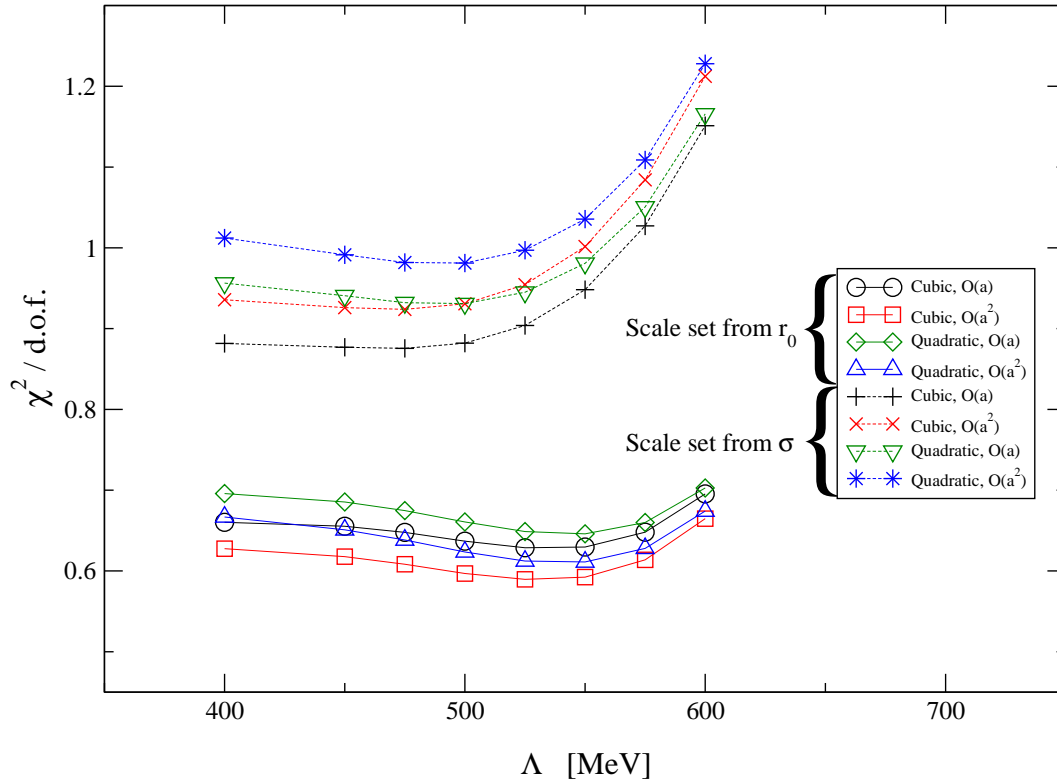


FIG. 8: A plot of  $\chi^2/d.o.f$  against  $\Lambda$  for the Gaussian form factor.

is another indication that there are  $\mathcal{O}(a)$  systematics present in the string tension data [28].

- *Setting the scale*

The  $\chi^2/d.o.f.$  using  $r_0$  are significantly lower than the  $\sigma$  fits, independent of whether the Adelaide or naive fits were used. In our study of the vector meson [28] we found this to be true for the Adelaide fits, whereas the naive fits had no preference either way for  $r_0$  or  $\sigma$ .

From Figs. 7 and 8 and Tables VI and VII, we see that the best fit choice is the dipole form factor using the cubic chiral expansion with  $\mathcal{O}(a^2)$  effects in the  $a_0$  coefficient and using  $r_0$  to set the scale. This choice will be used in the next section to determine the central value of our nucleon mass prediction and the spread from the other fitting types will be used to define the error.

Form Factor	Chiral Expansion	Lattice Spacing	$\Lambda_{\text{best}}$ [MeV]
Dipole	Cubic	$r_0$	$594^{+32}_{-59}$
”	”	$\sigma$	523
”	Quadratic	$r_0$	600
”	”	$\sigma$	550
Gaussian	Cubic	$r_0$	525
”	”	$\sigma$	475
”	Quadratic	$r_0$	550
”	”	$\sigma$	500

TABLE V: The best  $\Lambda$  values for each of the Adelaide fits from figs. 7 and 8. Note that best  $\Lambda$  values do not depend on whether  $\mathcal{O}(a)$  or  $\mathcal{O}(a^2)$  corrections in the  $a_0$  coefficient are used.

## V. PHYSICAL PREDICTIONS

In this section we extract a value for the continuum nucleon mass,  $M_N$ , in the limit of physical, degenerate quark masses. We also list the renormalised coefficients (i.e. low energy constants in the chiral expansion of the nucleon mass). All our predictions will obviously come from the global fit approach of sec. IV C, since this is a much more highly constrained method than the alternative method of sec. IV B. We obtain our predictions of  $M_N$  by setting  $M_{PS}^{deg} = M_{PS}^{non-deg} = M_{PS}^{unit} = \mu_\pi$  in Eqs. (15, 16 & 3) with  $\mu_\pi$  being the physical pion mass, which we take to be 138 MeV. We also set  $M_N^{deg} = M_N^{non-deg}$  and  $M_\Delta^{deg} = M_\Delta^{non-deg}$  in Eq. (3). In doing this we see that the  $\eta'$  contributions to the total self-energy (see Eqs. (2 & 3)) disappear in this continuum, physical case as required. The only remaining term involving  $M_N$  and  $M_\Delta$  is the  $\sigma_{N\Delta}^\pi$  self-energy term in which we set the mass splitting equal to the physical mass splitting of the nucleon and  $\Delta$  (i.e., 293 MeV [33]).

We make a physical prediction for each different fitting method (Table IV) using the coefficients ( $a_0^{cont}$ ,  $a_2$ ,  $a_4$  &  $a_6$ ) in Tables VI and VII for the sixteen Adelaide and eight naive

Fit Approach	Form Factor	$a_0^{cont}$ [GeV]	$X_1$ [GeVfm <sup>-1</sup> ]	$X_2$ [GeVfm <sup>-2</sup> ]	$a_2$ [GeV <sup>-1</sup> ]	$a_4$ [GeV <sup>-3</sup> ]	$a_6$ [GeV <sup>-5</sup> ]	$\chi^2/d.o.f.$
Cubic chiral extrapolation			$a_0$ contains $\mathcal{O}(a)$					
Adelaide	dipole	$1.08_{-2}^{+2}$	$-0.23_{-3}^{+2}$	-	$1.20_{-9}^{+9}$	$-0.5_{-2}^{+2}$	$0.17_{-9}^{+9}$	41 / 75
Adelaide	Gaussian	$1.08_{-2}^{+2}$	$-0.22_{-3}^{+2}$	-	$1.19_{-9}^{+10}$	$-0.5_{-2}^{+2}$	$0.16_{-9}^{+9}$	47 / 75
Naive	-	$1.02_{-2}^{+2}$	$-0.27_{-3}^{+2}$	-	$1.29_{-9}^{+10}$	$-0.6_{-2}^{+2}$	$0.21_{-9}^{+9}$	45 / 75
Cubic chiral extrapolation			$a_0$ contains $\mathcal{O}(a^2)$					
Adelaide	dipole	$1.060_{-16}^{+14}$	-	$-0.62_{-8}^{+6}$	$1.21_{-8}^{+10}$	$-0.53_{-18}^{+15}$	$0.17_{-8}^{+9}$	39 / 75
Adelaide	Gaussian	$1.059_{-16}^{+14}$	-	$-0.60_{-8}^{+6}$	$1.19_{-8}^{+10}$	$-0.51_{-18}^{+15}$	$0.16_{-8}^{+9}$	44 / 75
Naive	-	$0.999_{-17}^{+13}$	-	$-0.74_{-8}^{+6}$	$1.30_{-8}^{+10}$	$-0.64_{-18}^{+15}$	$0.22_{-8}^{+9}$	44 / 75
Quadratic chiral extrapolation			$a_0$ contains $\mathcal{O}(a)$					
Adelaide	dipole	$1.106_{-8}^{+7}$	$-0.23_{-3}^{+2}$	-	$1.03_{-2}^{+2}$	$-0.210_{-17}^{+15}$	-	43 / 76
Adelaide	Gaussian	$1.101_{-8}^{+7}$	$-0.22_{-3}^{+2}$	-	$1.03_{-2}^{+2}$	$-0.207_{-17}^{+15}$	-	49 / 76
Naive	-	$1.056_{-8}^{+7}$	$-0.28_{-3}^{+2}$	-	$1.07_{-2}^{+2}$	$-0.230_{-17}^{+15}$	-	49 / 76
Quadratic chiral extrapolation			$a_0$ contains $\mathcal{O}(a^2)$					
Adelaide	dipole	$1.088_{-7}^{+6}$	-	$-0.63_{-8}^{+6}$	$1.03_{-2}^{+2}$	$-0.209_{-17}^{+15}$	-	42 / 76
Adelaide	Gaussian	$1.084_{-7}^{+6}$	-	$-0.61_{-8}^{+6}$	$1.03_{-2}^{+2}$	$-0.206_{-17}^{+15}$	-	47 / 76
Naive	-	$1.034_{-7}^{+6}$	-	$-0.75_{-8}^{+6}$	$1.07_{-2}^{+2}$	$-0.230_{-17}^{+15}$	-	48 / 76

TABLE VI: The results of the global fit analysis where the scale is set from  $r_0$ .

fit cases. For the Adelaide fits, we use the relevant preferred value of  $\Lambda$  taken from Table V. We list these predictions for  $M_N$  in Table VIII.

In Figs. 9 and 10 we present a graphical representation of our study of the  $\Lambda$  dependence of  $M_N$  for both the dipole and Gaussian form factors. For the dipole case, we include the acceptable range for the  $\Lambda$  parameter which is represented by two vertical dashed lines. This range is defined from our plots of  $\chi^2/d.o.f$  against  $\Lambda$  (Figs. 7 & 8) by increasing  $\chi^2$  from its

Fit Approach	Form Factor	$a_0^{cont}$ [GeV]	$X_1$ [GeVfm <sup>-1</sup> ]	$X_2$ [GeVfm <sup>-2</sup> ]	$a_2$ [GeV <sup>-1</sup> ]	$a_4$ [GeV <sup>-3</sup> ]	$a_6$ [GeV <sup>-5</sup> ]	$\chi^2/d.o.f.$
		Cubic chiral extrapolation			$a_0$ contains $\mathcal{O}(a)$			
Adelaide	dipole	1.001 <sup>+15</sup> <sub>-14</sub>	-0.18 <sup>+2</sup> <sub>-2</sub>	-	1.32 <sup>+9</sup> <sub>-9</sub>	-0.7 <sup>+2</sup> <sub>-2</sub>	0.28 <sup>+10</sup> <sub>-10</sub>	61 / 75
Adelaide	Gaussian	1.002 <sup>+14</sup> <sub>-14</sub>	-0.17 <sup>+2</sup> <sub>-2</sub>	-	1.30 <sup>+9</sup> <sub>-8</sub>	-0.7 <sup>+2</sup> <sub>-2</sub>	0.27 <sup>+10</sup> <sub>-10</sub>	66 / 75
Naive	-	0.966 <sup>+15</sup> <sub>-14</sub>	-0.21 <sup>+2</sup> <sub>-2</sub>	-	1.39 <sup>+9</sup> <sub>-9</sub>	-0.8 <sup>+2</sup> <sub>-2</sub>	0.33 <sup>+10</sup> <sub>-10</sub>	62 / 75
		Cubic chiral extrapolation			$a_0$ contains $\mathcal{O}(a^2)$			
Adelaide	dipole	0.986 <sup>+12</sup> <sub>-14</sub>	-	-0.48 <sup>+6</sup> <sub>-6</sub>	1.32 <sup>+9</sup> <sub>-8</sub>	-0.7 <sup>+2</sup> <sub>-2</sub>	0.29 <sup>+10</sup> <sub>-9</sub>	66 / 75
Adelaide	Gaussian	0.988 <sup>+12</sup> <sub>-14</sub>	-	-0.44 <sup>+6</sup> <sub>-6</sub>	1.30 <sup>+9</sup> <sub>-8</sub>	-0.7 <sup>+2</sup> <sub>-2</sub>	0.28 <sup>+10</sup> <sub>-9</sub>	69 / 75
Naive	-	0.947 <sup>+13</sup> <sub>-14</sub>	-	-0.56 <sup>+6</sup> <sub>-6</sub>	1.39 <sup>+9</sup> <sub>-8</sub>	-0.8 <sup>+2</sup> <sub>-2</sub>	0.33 <sup>+10</sup> <sub>-9</sub>	68 / 75
		Quadratic chiral extrapolation			$a_0$ contains $\mathcal{O}(a)$			
Adelaide	dipole	1.036 <sup>+7</sup> <sub>-7</sub>	-0.19 <sup>+2</sup> <sub>-2</sub>	-	1.08 <sup>+2</sup> <sub>-2</sub>	-0.24 <sup>+2</sup> <sub>-2</sub>	-	67 / 76
Adelaide	Gaussian	1.036 <sup>+7</sup> <sub>-7</sub>	-0.17 <sup>+2</sup> <sub>-2</sub>	-	1.08 <sup>+2</sup> <sub>-2</sub>	-0.23 <sup>+2</sup> <sub>-2</sub>	-	71 / 76
Naive	-	1.006 <sup>+6</sup> <sub>-7</sub>	-0.22 <sup>+2</sup> <sub>-2</sub>	-	1.11 <sup>+2</sup> <sub>-2</sub>	-0.26 <sup>+2</sup> <sub>-2</sub>	-	69 / 76
		Quadratic chiral extrapolation			$a_0$ contains $\mathcal{O}(a^2)$			
Adelaide	dipole	1.020 <sup>+6</sup> <sub>-6</sub>	-	-0.49 <sup>+6</sup> <sub>-6</sub>	1.08 <sup>+2</sup> <sub>-2</sub>	-0.23 <sup>+2</sup> <sub>-2</sub>	-	71 / 76
Adelaide	Gaussian	1.021 <sup>+6</sup> <sub>-6</sub>	-	-0.46 <sup>+6</sup> <sub>-6</sub>	1.07 <sup>+2</sup> <sub>-2</sub>	-0.23 <sup>+2</sup> <sub>-2</sub>	-	75 / 76
Naive	-	0.987 <sup>+6</sup> <sub>-6</sub>	-	-0.58 <sup>+6</sup> <sub>-6</sub>	1.11 <sup>+2</sup> <sub>-2</sub>	-0.25 <sup>+2</sup> <sub>-2</sub>	-	75 / 76

TABLE VII: The results of the global fit analysis where the scale is set from  $\sigma$ .

minimum by unity.

We summarise the results of this section which are outlined in Table VIII and figures 9 and 10 below.

- The statistical errors in the mass estimates are typically less than 1% for the quadratic extrapolations and less than 2% for the cubic extrapolations.
- We see disagreement between all types of fit when different methods are used to set

Estimate	Form	$M_N$ [GeV]	$M_N$ [GeV]
Approach	Factor	(Scale from $r_0$ )	(Scale from $\sigma$ )
Experimental	-		0.939
Cubic chiral extrapolation		$a_0$ contains $\mathcal{O}(a)$	
Adelaide	dipole	$0.984^{+15}_{-15}$	$0.950^{+13}_{-13}$
Adelaide	Gaussian	$0.973^{+15}_{-15}$	$0.938^{+12}_{-13}$
Naive	-	$1.046^{+15}_{-15}$	$0.992^{+13}_{-13}$
Cubic chiral extrapolation		$a_0$ contains $\mathcal{O}(a^2)$	
Adelaide	dipole	$0.965^{+12}_{-15}$	$0.934^{+11}_{-12}$
Adelaide	Gaussian	$0.956^{+12}_{-15}$	$0.923^{+11}_{-12}$
Naive	-	$1.023^{+12}_{-15}$	$0.974^{+11}_{-12}$
Quadratic chiral extrapolation		$a_0$ contains $\mathcal{O}(a)$	
Adelaide	dipole	$1.006^{+7}_{-8}$	$0.974^{+6}_{-6}$
Adelaide	Gaussian	$0.986^{+7}_{-8}$	$0.959^{+6}_{-6}$
Naive	-	$1.076^{+7}_{-8}$	$1.027^{+6}_{-6}$
Quadratic chiral extrapolation		$a_0$ contains $\mathcal{O}(a^2)$	
Adelaide	dipole	$0.988^{+6}_{-7}$	$0.958^{+5}_{-6}$
Adelaide	Gaussian	$0.969^{+6}_{-7}$	$0.945^{+5}_{-6}$
Naive	-	$1.054^{+6}_{-7}$	$1.008^{+5}_{-6}$

TABLE VIII: Estimates of  $M_N$  obtained from the global fits. (The errors are statistical only.) Our experimental estimate comes from a simple average of the proton and neutron masses.



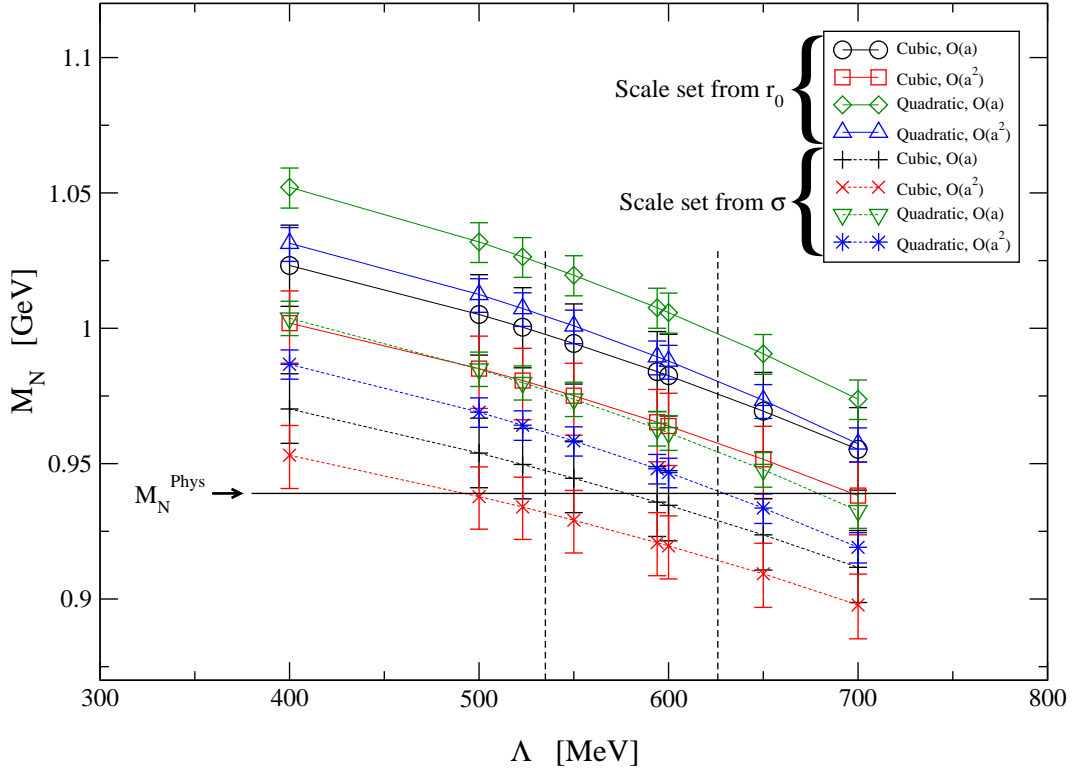


FIG. 9: A plot of  $M_N$  as a function of  $\Lambda$  from the Adelaide approach using a dipole form factor. Recall that the best  $\Lambda$  value when the scale is set from  $r_0$  for the dipole form factor is  $\Lambda = 594$  MeV. The two vertical dashed lines define the range of acceptable  $\Lambda$  values ( $535 \text{ MeV} \leq \Lambda \leq 626$  MeV) obtained by increasing  $\chi^2$  by unity in Fig. 7.

the scale. When the scale is set from  $r_0$  the mass predictions are always higher than when the scale is set from  $\sigma$ .

- We also see that the  $M_N$  predictions within one particular method (i.e. the Adelaide dipole, Adelaide Gaussian or naive method) have a variation in the results of between 3% and 5%, with the largest variation in the naive mass predictions. This disagreement suggests some instability in the fits, possibly because the lattice systematics are more complicated than we have assumed.
- The Adelaide method always produces a mass prediction closer to the physical nucleon mass. For the cubic fits the Adelaide mass predictions are very accurate compared to their naive counterparts. They are typically within two statistical error bars of the experimental mass.

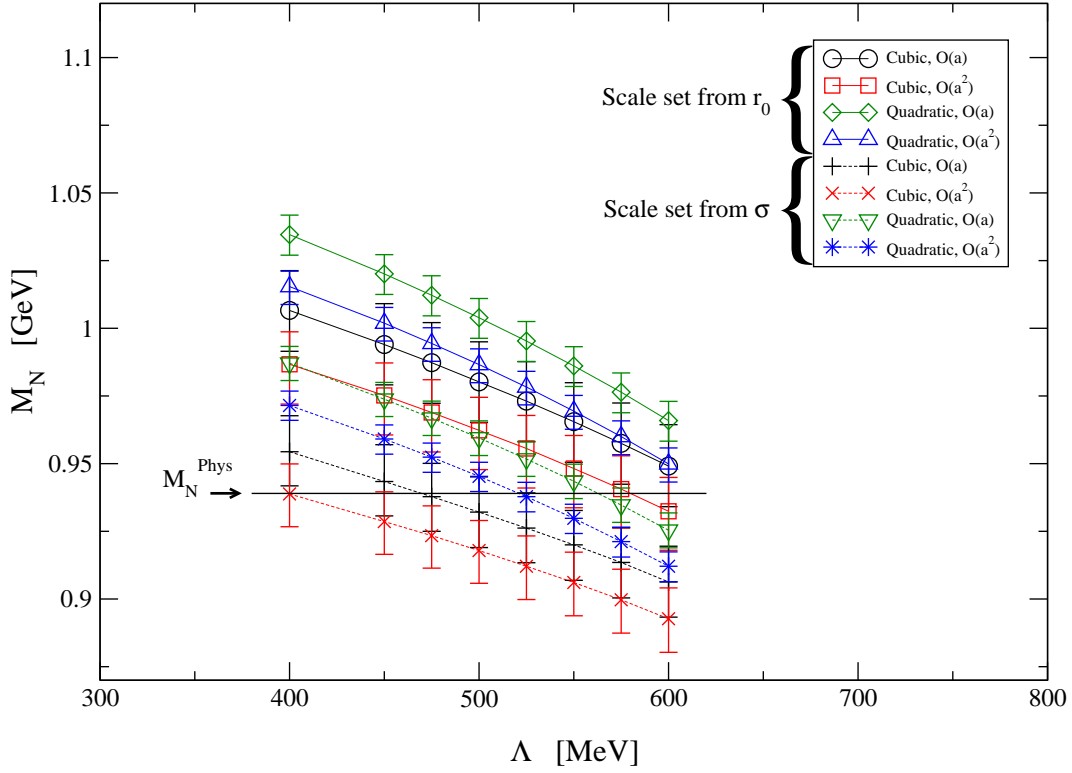


FIG. 10: A plot of  $M_N$  as a function of  $\Lambda$  from the Adelaide approach using a Gaussian form factor. Recall that the best  $\Lambda$  value when the scale is set from  $r_0$  for the Gaussian form factor is  $\Lambda = 525$  MeV.

- The variation of  $M_N$  in the region of allowed values of  $\Lambda$  is very small for each different fit. Typically of the order of the other uncertainties.

As with the results of the meson study [28] we conclude by noting all of these points favour the Adelaide approach over the naive method. This suggests that the Adelaide method should be the preferred method when performing chiral extrapolations and is a significant improvement over the naive method. To give the final value for  $M_N$  for both the Adelaide method and the naive method, we use our preferred choices: the cubic chiral extrapolation with  $\mathcal{O}(a^2)$  corrections in  $a_0$ ;  $r_0$  to set the scale; and, for the Adelaide method we use the dipole form factor. We quote an error that is based on the spread in the mass predictions (for the  $r_0$  case only). We also (for the Adelaide method) include an estimate of the error associated with the  $\Lambda$  parameter which is taken from the vertical dashed lines in Fig. 9.

Hence our final mass estimate for the nucleon is

$$M_N^{Adelaide} = 965(15)_{-0}^{+41+13}\text{MeV} \quad (17)$$

$$M_N^{Naive} = 1023(15)_{-0}^{+53}\text{MeV} \quad (18)$$

where the first error is statistical and the second is taken from the fit procedure. The third error in the Adelaide case is due to the  $\Lambda$  parameter. We have not considered any error that may be associated with the determination of  $r_0$  which we take to be 0.49 fm. We note that the Adelaide central value would be  $1\sigma$  (of the combined in quadrature errors) away from experiment by simply rescaling  $r_0$  upwards from 0.49 fm by around 1%. This corresponds exactly with what we found in the  $\rho$ -meson mass case [28]. However, other results have hinted at smaller values of  $r_0$  [35–37]. To a good approximation, the  $M_N$  estimates for these values of  $r_0$  near 0.49fm can be obtained by a simple scaling of the values in Eqs.(17 & 18).

We now turn to the renormalised coefficients,  $c_{0,2}$ , which are defined from Eqs.(2 & 11).

$$\begin{aligned} M_N &= a_0 + a_2(M_{PS}^{deg})^2 + a_4(M_{PS}^{deg})^4 + \sigma_{NN}^\pi + \sigma_{N\Delta}^\pi + \dots \\ &\equiv a_0 + a_2(M_{PS}^{deg})^2 + a_4(M_{PS}^{deg})^4 \\ &\quad + (a_{NN}^\pi)^{(0)} + (a_{NN}^\pi)^{(2)}(M_{PS}^{deg})^2 + c_{LNA}(M_{PS}^{deg})^3 \\ &\quad + (a_{N\Delta}^\pi)^{(0)} + (a_{N\Delta}^\pi)^{(2)}(M_{PS}^{deg})^2 + c_{NLNA}(M_{PS}^{deg})^4 \ln(M_{PS}^{deg}) + \dots \\ &\equiv c_0 + c_2(M_{PS}^{deg})^2 + c_4(M_{PS}^{deg})^4 \\ &\quad + c_{LNA}(M_{PS}^{deg})^3 + c_{NLNA}(M_{PS}^{deg})^4 \ln(M_{PS}^{deg}) + \dots \end{aligned} \quad (19)$$

Again we have used the fact that the  $\eta'$  terms,  $\sigma_{NN}^{\eta'}$  and  $\sigma_{N\Delta}^{\eta'}$ , disappear in the continuum, physical case, and we note that the  $\sigma_{NN}^\pi, \sigma_{N\Delta}^\pi$  contributions reproduce the LNA and NLNA terms respectively once they are chirally expanded. By expanding  $\sigma_{NN}^\pi$  and  $\sigma_{N\Delta}^\pi$  (from eq.(3)) about  $M_{PS}^2 = 0$  we obtain the values for  $(a_{NN}^\pi)^{(0,2)}$  and  $(a_{N\Delta}^\pi)^{(0,2)}$  listed in Tables IX and X. Note that these values correspond to the fit procedures used in Tables VI and VII. The  $\Lambda$  values used are those in Table V. From eq(19) we have

$$c_{0,2} = a_{0,2} + (a_{NN}^\pi)^{(0,2)} + (a_{N\Delta}^\pi)^{(0,2)}. \quad (20)$$

Tables IX and X list the values of  $c_{0,2}$  for each of the fit procedures. Using the same preferred fitting method as in the nucleon mass case (cubic chiral extrapolation with  $\mathcal{O}(a^2)$  corrections in  $a_0$  with  $r_0$  to set the scale and using the dipole form factor) we obtain

$$c_0 = 0.930(16)_{-12}^{+42}\text{GeV} \quad c_2 = 2.61(10)_{-17}^{+17}\text{GeV}^{-1}, \quad (21)$$

where the first error is statistical and the second is from the fit procedure. The  $c_0$  value is very close to the experimental value of  $M_N$  as expected. Furthermore, the  $c_2$  value compares very favourably with [3] who obtained  $c_2 = 2.80(33)(35) \text{ GeV}^{-1}$  (where we note the statistical error in [3] was reported at  $2\sigma$ ). Note however that this was with full, 2-flavour QCD (rather than pQQCD); the reduced error in our case is due to the larger dataset generically available in pQQCD. Other work, [34], calculates a similar quantity they call  $c_1$  from low energy  $\pi - N$  fits. This is related to our  $c_2$  via

$$c_1 \equiv -c_2/4. \quad (22)$$

[34] obtains  $c_1 = -0.9^{+0.5}_{-0.2} \text{ GeV}^{-1}$ , which, using eq.(22), predicts  $c_2 = 3.6^{+0.8}_{-2.0} \text{ GeV}^{-1}$ . Again, this estimate is consistent with our result in eq(21), but with significantly larger errors. Note however, that the result from [34] uses experimental (2+1 flavour) data. Thus it is clear that there is significant benefit in simulating pQQCD since it generates a larger dataset which results in a corresponding reduction in the errors associated with physical predictions and low energy constants.

## VI. CONCLUSIONS

While the computing resources needed to generate gauge configurations with dynamical fermions are very significant, the computation of hadron properties with different valence quark masses is relatively low cost for any given sea quark mass. Thus, if one can deal with the effects of partial quenching in a controlled manner, this approach offers a potentially cost effective way to increase the statistical precision of the final, physical results. This philosophy has already been successfully applied to the mass of the  $\rho$  meson in earlier work [28]. Here, we have estimated the nucleon mass and its corresponding low energy constants from a large CP-PACS simulation [1] of partially-quenched baryon masses using the Adelaide chiral extrapolation approach. We have shown that this method is a valid approach to the study of the chiral properties of the nucleon mass in the partially-quenched theory. As a comparison, we have also used a naive (polynomial) fitting procedure, but found that it is a much poorer predictor of the experimental number compared with the Adelaide approach. Our predictions from both methods are given in Eqs. (17 & 18).

We have shown that a single global fit of all 80 degenerate nucleon mass points from [1] at different valence and sea quark masses, and at different lattice spacings is possible using the Adelaide approach. This fit procedure has only 5 fit parameters and includes chiral effects,

Form Factor	$(a_{NN}^\pi)^{(0)}$ [GeV]	$(a_{N\Delta}^\pi)^{(0)}$ [GeV]	$c_0$ [GeV]	$(a_{NN}^\pi)^{(2)}$ [GeV <sup>-1</sup> ]	$(a_{N\Delta}^\pi)^{(2)}$ [GeV <sup>-1</sup> ]	$c_2$ [GeV <sup>-1</sup> ]
Cubic chiral extrapolation			$a_0$ contains $\mathcal{O}(a)$			
dipole	-0.074	-0.056	$0.95_{-2}^{+2}$	1.056	0.339	$2.60_{-9}^{+9}$
Gaussian	-0.082	-0.059	$0.94_{-2}^{+2}$	1.191	0.401	$2.78_{-9}^{+10}$
Cubic chiral extrapolation			$a_0$ contains $\mathcal{O}(a^2)$			
dipole	-0.074	-0.056	$0.930_{-16}^{+14}$	1.056	0.339	$2.61_{-8}^{+10}$
Gaussian	-0.082	-0.059	$0.918_{-16}^{+14}$	1.191	0.401	$2.78_{-8}^{+10}$
Quadratic chiral extrapolation			$a_0$ contains $\mathcal{O}(a)$			
dipole	-0.077	-0.058	$0.972_{-8}^{+7}$	1.066	0.345	$2.44_{-2}^{+2}$
Gaussian	-0.094	-0.069	$0.938_{-8}^{+7}$	1.248	0.433	$2.71_{-2}^{+2}$
Quadratic chiral extrapolation			$a_0$ contains $\mathcal{O}(a^2)$			
dipole	-0.077	-0.058	$0.954_{-7}^{+6}$	1.066	0.345	$2.44_{-2}^{+2}$
Gaussian	-0.094	-0.069	$0.921_{-7}^{+6}$	1.248	0.433	$2.71_{-2}^{+2}$

TABLE IX: The renormalised coefficients  $c_{0,2}$  using the scale set from  $r_0$ .

finite volume and finite lattice spacing effects. The only systematic deviation from nature not included is the number of sea quark flavours which is two in the CP-PACS simulation. The Adelaide method includes a form factor and an associated scale,  $\Lambda$ . In this work, we have shown that both the type of form factor, and the preferred value of  $\Lambda$  can be determined. As a by-product, we have been able to determine the low energy constant in the chiral expansion of the nucleon mass,  $c_2$ , to a remarkable level of accuracy (see eq.(21)). Again this emphasises the benefits that can be obtained from the larger dataset that pQQCD data affords.

Form Factor	$(a_{NN}^\pi)^{(0)}$ [GeV]	$(a_{N\Delta}^\pi)^{(0)}$ [GeV]	$c_0$ [GeV]	$(a_{NN}^\pi)^{(2)}$ [GeV <sup>-1</sup> ]	$(a_{N\Delta}^\pi)^{(2)}$ [GeV <sup>-1</sup> ]	$c_2$ [GeV <sup>-1</sup> ]
Cubic chiral extrapolation			$a_0$ contains $\mathcal{O}(a)$			
dipole	-0.051	-0.036	$0.914^{+15}_{-14}$	0.929	0.273	$2.52^{+9}_{-9}$
Gaussian	-0.061	-0.042	$0.900^{+14}_{-14}$	1.078	0.338	$2.72^{+9}_{-8}$
Cubic chiral extrapolation			$a_0$ contains $\mathcal{O}(a^2)$			
dipole	-0.051	-0.036	$0.899^{+12}_{-14}$	0.929	0.273	$2.52^{+9}_{-8}$
Gaussian	-0.061	-0.042	$0.886^{+12}_{-14}$	1.078	0.338	$2.72^{+9}_{-8}$
Quadratic chiral extrapolation			$a_0$ contains $\mathcal{O}(a)$			
dipole	-0.059	-0.043	$0.934^{+7}_{-7}$	0.977	0.298	$2.36^{+2}_{-2}$
Gaussian	-0.071	-0.050	$0.915^{+7}_{-7}$	1.134	0.369	$2.58^{+2}_{-2}$
Quadratic chiral extrapolation			$a_0$ contains $\mathcal{O}(a^2)$			
dipole	-0.059	-0.043	$0.918^{+6}_{-6}$	0.977	0.298	$2.36^{+2}_{-2}$
Gaussian	-0.071	-0.050	$0.900^{+6}_{-6}$	1.134	0.369	$2.57^{+2}_{-2}$

TABLE X: The renormalised coefficients  $c_{0,2}$  using the scale set from  $\sigma$ .

### Acknowledgements

CRA and WA would like to thank the CSSM for their support and kind hospitality. WA would like to thank PPARC for travel support. The authors would like to thank Stewart Wright for helpful comments. This work is supported by the Australian Research Council and by U.S. DOE Contract No. DE-AC05-06OR23177, under which Jefferson Science Associates, LLC operates Jefferson Laboratory, and DE-AC02-06CH11357, under which UChicago Ar-

gonne, LLC operates Argonne National Laboratory.

---

- [1] A. Ali Khan *et al.* [CP-PACS Collaboration], Phys. Rev. D **65**, 054505 (2002) [Erratum-ibid. D **67**, 059901 (2003)] [arXiv:hep-lat/0105015].
- [2] K. Jansen, PoS **LATTICE2008** (2008) 010 [arXiv:0810.5634 [hep-lat]].
- [3] D. B. Leinweber, A. W. Thomas and R. D. Young, Phys. Rev. Lett. **92** (2004) 242002 [arXiv:hep-lat/0302020].
- [4] M. Procura, T. R. Hemmert and W. Weise, Phys. Rev. D **69**, 034505 (2004) [arXiv:hep-lat/0309020].
- [5] D. B. Leinweber, A. W. Thomas and R. D. Young, Phys. Rev. Lett. **86**, 5011 (2001) [arXiv:hep-ph/0101211].
- [6] D. B. Leinweber, A. W. Thomas, K. Tsushima and S. V. Wright, Phys. Rev. D **61**, 074502 (2000) [arXiv:hep-lat/9906027].
- [7] C. Bernard, S. Hashimoto, D. B. Leinweber, P. Lepage, E. Pallante, S. R. Sharpe and H. Wittig, Nucl. Phys. Proc. Suppl. **119**, 170 (2003) [arXiv:hep-lat/0209086].
- [8] R. D. Young, D. B. Leinweber and A. W. Thomas, Prog. Part. Nucl. Phys. **50**, 399 (2003) [arXiv:hep-lat/0212031].
- [9] S. Durr, Eur. Phys. J. C **29**, 383 (2003) [arXiv:hep-lat/0208051].
- [10] S. R. Beane, Nucl. Phys. B **695**, 192 (2004) [arXiv:hep-lat/0403030].
- [11] A. W. Thomas, P. A. M. Guichon, D. B. Leinweber and R. D. Young, Prog. Theor. Phys. Suppl. **156**, 124 (2004) [arXiv:nucl-th/0411014].
- [12] D. B. Leinweber, A. W. Thomas and R. D. Young, Nucl. Phys. A **755**, 59 (2005) [arXiv:hep-lat/0501028].
- [13] J. A. McGovern and M. C. Birse, Phys. Rev. D **74** (2006) 097501 [arXiv:hep-lat/0608002].
- [14] J. F. Donoghue, B. R. Holstein and B. Borasoy, Phys. Rev. D **59**, 036002 (1999) [arXiv:hep-ph/9804281].
- [15] D. Djukanovic, M. R. Schindler, J. Gegelia and S. Scherer, Phys. Rev. D **72**, 045002 (2005).
- [16] R. D. Young, D. B. Leinweber and A. W. Thomas, Phys. Rev. D **71**, 014001 (2005) [arXiv:hep-lat/0406001].
- [17] M. F. L. Golterman and K. C. L. Leung, Phys. Rev. D **57**, 5703 (1998) [arXiv:hep-lat/9711033].

- [18] S. R. Sharpe and N. Shoresh, Phys. Rev. D **64**, 114510 (2001) [arXiv:hep-lat/0108003].
- [19] J. W. Chen and M. J. Savage, Phys. Rev. D **65**, 094001 (2002) [arXiv:hep-lat/0111050].
- [20] S. R. Beane and M. J. Savage, Nucl. Phys. A **709**, 319 (2002) [arXiv:hep-lat/0203003].
- [21] D. B. Leinweber, Phys. Rev. D **69**, 014005 (2004) [arXiv:hep-lat/0211017].
- [22] D. B. Leinweber *et al.*, Phys. Rev. Lett. **94**, 212001 (2005) [arXiv:hep-lat/0406002].
- [23] D. B. Leinweber *et al.*, Phys. Rev. Lett. **97**, 022001 (2006) [arXiv:hep-lat/0601025].
- [24] D. Arndt and B. C. Tiburzi, Phys. Rev. D **68**, 094501 (2003) [arXiv:hep-lat/0307003].
- [25] D. Arndt and C.-J. D. Lin, Phys. Rev. D **70**, 014503 (2004) [arXiv:hep-lat/0403012].
- [26] J. Bijnens, N. Danielsson and T. A. Lahde, Phys. Rev. D **70**, 111503 (2004) [arXiv:hep-lat/0406017].
- [27] W. Detmold and C. J. Lin, Phys. Rev. D **71**, 054510 (2005) [arXiv:hep-lat/0501007].
- [28] C.R.Allton, W. Armour, D.B.Leinweber, A.W.Thomas, R.D.Young, Phys.Lett.**B628** (2005) 125 [arXiv:hep-lat/0504022]; W. Armour, C.R. Allton, D.B. Leinweber, A.W. Thomas and R. Young, J. Phys. G: Nucl. Part. Phys. **32** (2006) 971-991., [arXiv:hep-lat/0510078].
- [29] D. B. Leinweber and T. D. Cohen, Phys. Rev. D **49** (1994) 3512 [arXiv:hep-ph/9307261].
- [30] R. D. Young, D. B. Leinweber, A. W. Thomas and S. V. Wright, Phys. Rev. D **66**, 094507 (2002) [arXiv:hep-lat/0205017].
- [31] Malcolm Butler, Martin Savage, Roxanne Springer., Nucl.Phys. **B399** (1993) 69-88 [arXiv:hep-ph/9211247].
- [32] B. Borasoy., Phys.Rev. **D59** (1999) 054021.
- [33] C. Amsler *et al.* [Particle Data Group], Phys. Lett. B **667**, 1 (2008).
- [34] U. G. Meissner, Nucl. Phys. Proc. Suppl. **153** (2006) 170.
- [35] C. Aubin *et al.*, Phys. Rev. D **70** (2004) 094505 [arXiv:hep-lat/0402030].
- [36] A. A. Khan *et al.*, Phys. Rev. D **74** (2006) 094508 [arXiv:hep-lat/0603028].
- [37] P. Boucaud *et al.* [ETM Collaboration], Phys. Lett. B **650** (2007) 304 [arXiv:hep-lat/0701012].
- [38] For a full discussion see [31].
- [39] We take the values of  $m_\Sigma$  in table XXIII to be the mass values for the non-degenerate nucleon. We can do this since the interpolation operators for  $N$  and  $\Sigma$  have the same quantum numbers
- [40] We choose  $\mathcal{O}(a)$  and  $\mathcal{O}(a^2)$  corrections because the lattice action is tree-level improved and so should contain  $\mathcal{O}(a^2)$  errors together with some  $\mathcal{O}(a)$  errors.